Cloud top pressure retrieval with DSCOVR-EPIC oxygen A and B bands observation

Bangsheng Yin[1], Qilong Min[1, *], Emily Morgan[1], Yuekui Yang[2], Alexander Marshak[2], and Anthony B. Davis[3]

[1]Atmospheric Sciences Research Center, University at Albany, Albany, NY, USA

[2]NASA Goddard Space Flight Center, Climate and Radiation Laboratory, Greenbelt, MD, USA

[3]Jet Propulsion Laboratory, California Institute of Technology, Pasadena, CA, USA

[*] Corresponding author, qmin@albany.edu

Abstract

An analytic transfer inverse model for Earth Polychromatic Imaging Camera (EPIC) observation is proposed to retrieve the cloud top pressure (CTP) with considering in-cloud photon penetration. In this model, an analytic equation was developed to represent the reflection at top of atmosphere (TOA) from above cloud, in-cloud, and below-cloud. The coefficients of this analytic equation can be derived from a series of EPIC simulations under different atmospheric conditions using a non-linear regression algorithm. With estimated cloud pressure thickness, the CTP can be retrieved from EPIC observation data by solving the analytic equation. To simulate the EPIC measurements, a program package using the double-k approach was developed. Compared to line-by-line calculation, this approach can calculate high-accuracy results with a one-hundred-fold computation time reduction. During the retrieval processes, two kinds of retrieval results, i.e., baseline CTP and retrieved CTP, are provided. The baseline CTP is derived without considering in-cloud photon penetration, and the retrieved CTP is derived by solving the analytic equation, taking into consideration the in-cloud and below-cloud interactions. The retrieved CTP for the oxygen A and B bands are smaller than their related baseline CTP. At the same time, both baseline CTP and retrieved CTP at the oxygen B-band are larger than those at the oxygen A-band. Compared to the difference of baseline CTP between the B-band and A-band, the difference of retrieved CTP between these two bands is generally reduced. Out of around 10000 cases, in retrieved CTP between A- and B-bands we found an average bias of 93 mb with standard deviation of 81 mb. The cloud layer top pressure from Cloud-Aerosol Lidar and Infrared Pathfinder Satellite Observations measurements is used to do validation. Under single-layer cloud situations, the retrieved CTPs for the oxygen A-band agree well with the CTPs from CALIPSO, which mean difference is within 5 mb in the case study. Under multiple-layer cloud situations, the CTPs derived from EPIC measurements may be larger than the CTPs of high level thin-clouds due to the effect of photon penetration.

1. Introduction

The Deep-Space Climate Observatory (DSCOVR) satellite is an observation platform orbiting within the first Sun-Earth Lagrange point (L1), 1.5 million km from the Earth, carrying a suite of instruments oriented both Earthward and sunward. One of the Earthward instruments is the Earth Polychromatic Imaging Camera (EPIC) sensor, which can take images of the Earth with spatial resolution of 10 km at nadir. The EPIC continuously monitors the entire sunlit Earth for backscatter, with a nearly constant scattering angle between 168.5º and 175.5º, from sunrise to sunset with 10 narrowband filters: 317, 325, 340, 388, 443, 552, 680, 688, 764 and 779 nm (Marshak et al., 2018). Of the 10 narrow-band channels, there are two oxygen absorption and reference pairs, 764nm versus 779.5nm and 680nm versus 687.75nm, for oxygen A and B bands. The cloud top pressure (CTP) or cloud top height (CTH) is an important cloud property for climate and weather studies. Based on differential oxygen absorption, both EPIC oxygen A-band and B-band pairs can be used to retrieve CTP. It is worth noting that although CTP and CTH reference the same characteristic of clouds, the conversion between the two depends on the related atmospheric profile.

Although the theory of using oxygen absorption bands to retrieve CTP was proposed decades ago (Yamamoto and Wark, 1961), it is still very challenging to do the retrieval accurately due to the complicated in-cloud penetration effect (Yang et al., 2019, 2013; Davis et al., 2018a, 2018b; Richardson and Stephens, 2018; Loyola et al., 2018; Lelli et al., 2014, 2012; Schuessler et al., 2013; Rozanov and Kokhanovsky, 2004; Kokhanovsky and Rozanov, 2004; Kuze and Chance, 1994; O'brien and Mitchell, 1992; Fischer and Grassl, 1991; and etc.). To estimate the CTP from satellite measurements, many approaches have been designed to retrieve clouds' effective top pressures without considering in-cloud photon penetration. These approaches did not consider light penetrating cloud, therefore the derived CTH is lower than the cloud top, and the effective top pressures is higher than CTP. In the meantime, to improve the retrieval accuracy of CTP, various techniques have been applied to the retrieval methods with in-cloud photon penetration. For example, Kokhanovsky and Rozanov (2004) proposed a simple semi-analytical model for calculation of the top-of-atmosphere (TOA) reflectance of an underlying surface-atmosphere system, accounting both for aerosol and cloud scattering. Based on the work of Kokhanovsky and Rozanov (2004), Rozanov and Kokhanovsky (2004) developed an asymptotic algorithm for the CTH and the geometrical thickness determination using measurements of the cloud reflection function. This retrieval method was applied by Lelli et al. (2012, 2014) to derive CTH using measurements from GOME instrument on board the ESA ERS-2 space platform.

Currently, based on the measurements of DSCOVR EPIC sensor, the Atmospheric Science Data Center (ASDC) at National Aeronautics and Space Administration (NASA) Langley Research Center archives both calibrated EPIC reflectance ratio data and processed Level 2 cloud retrieval products, including cloud cover, cloud optical depth (COD), cloud effective top pressure at oxygen A and B bands (Yang et al., 2019). By using EPIC reflectance ratio data at oxygen A-band and B-band absorption to reference channels, Yang et al (2013) developed a method to retrieve CTH and cloud geometrical thickness simultaneously for fully cloudy scene over ocean surface. First their method calculates cloud centroid heights for both A- and B-band channels using the ratios between the reflectance of the absorption and reference channels, then derives the CTH and the cloud geometrical thickness from the two dimensional look up tables that relate the sum and the difference between the retrieved centroid heights for A- and B-bands

84 to the CTH and the cloud geometrical thickness. The difference in the O_2 A- and B-band cloud
85 centroid heights is resulted from the different penetration depths of the two bands. Compared to
86 the cloud height variability, the penetration depth differences are much smaller and the retrieval
87 accuracy from this method can be affected by the instrument noise (Davis et al. 2018a, b).

88   In this paper, to address the issue of in-cloud penetration, we proposed an analytic method
89 to retrieve the CTP by using DSCOVR EPIC oxygen A- and B-band observation. This analytical
90 method adopted ideas of the semi-analytical model (Kokhanovsky and Rozanov, 2004; Rozanov
91 and Kokhanovsky, 2004), and developed a quadratic EPIC analytic radiative transfer equation to
92 analyze the radiative transfer in oxygen A- and B-band channels. The structure of this paper is as
93 follows: section 2 describes the theory and methods, which includes several subsections, i.e., the
94 introduction of DSCOVR EPIC oxygen A and B bands filters, the theory of CTP retrieval based
95 on EPIC oxygen A- and B- band observation, and the detailed retrieval algorithm; section 3
96 describes the application and validation of the CTP retrieval method, which also includes several
97 subsections, i.e., case studies of CTP retrieval, validation of the retrieval method, and retrieval of
98 global observation; and section 4 states the conclusions of this study.

99

100 **2. Theory and methods**

101 **2.1 DSCOVR EPIC oxygen A and B bands filters**

102   EPIC filters at 764 nm and 779 nm cover the oxygen A-band absorption and reference
103 bands, respectively (Figure 1a). The high resolution absorption optical depth spectrum at oxygen
104 A-band and B-band is calculated by Line-By-Line Radiative Transfer Model (LBLRTM, Clough
105 et al., 2005) with HITRAN 2016 database (Gordon et al., 2017) for the U.S. standard
106 atmosphere. In this wavelength range, the O3 absorption is very weak (O3 optical depth < 0.003)
107 and there are no other gas absorptions. The background aerosol and Rayleigh scattering optical
108 depth vary smoothly within the A-band range; the differences between in-band and reference
109 band are negligible at nominal EPIC response functions. EPIC filters at 688 nm and 680 nm
110 cover the oxygen B-band absorption and reference band, respectively (Figure 1b). Compared to
111 the oxygen A-band, O3 absorption is slightly stronger in the oxygen B-band range, with an O3
112 optical depth around 0.01. Any water vapor absorption in the B-band range is negligible. In the
113 standard atmospheric model, from the oxygen B-band reference band to the absorption band, the
114 O3 absorption and Rayleigh scattering optical depth decreased by approximately 0.002 and
115 0.002, respectively. This may have some impacts on the CTP retrieval from the oxygen B-band
116 (more discussion in the later sections). It is worth noting that for EPIC measurements at both
117 oxygen A- and B-bands, the surface influence cannot be ignored. For examples, in the snow or
118 ice covered area the surface albedo is high; in the plants covered area, the surface albedo changes
119 substantially between oxygen A-band and B-band due to the impact of spectral red-edge (Seager
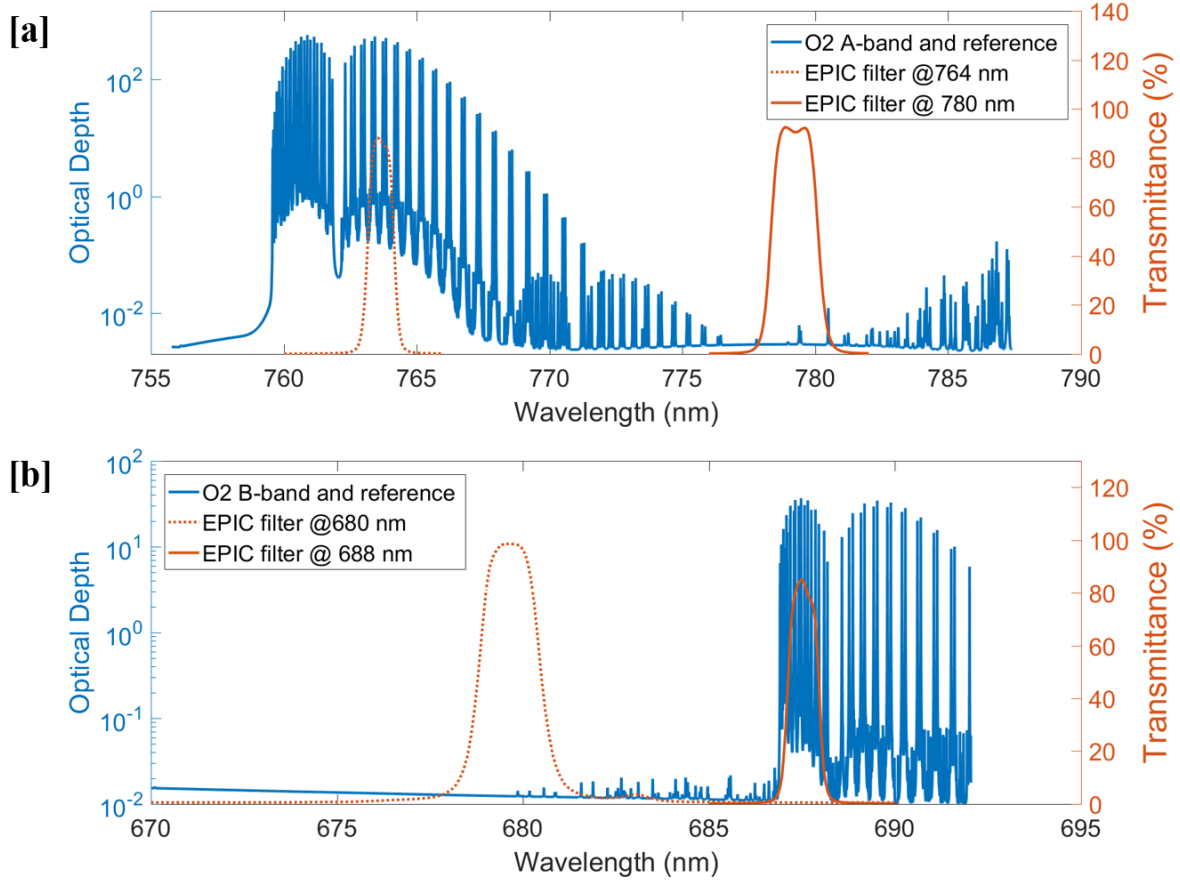120 et al., 2005).

Figure 1: High resolution calculated absorption optical depth spectrum at oxygen A-band (a) and B-band (b) with DSCOVR EPIC oxygen A and B bands in-band and reference filters. Here the absorption optical depth spectrum is calculated by LBLRTM model with HITRAN 2016 database for the U.S. standard atmosphere.

In general, if we use the pair of oxygen A and B absorption and reference bands together, the impact of other absorption lines, background Rayleigh scattering, and aerosol optical depth are very limited. At the same time, as a well-mixed major atmospheric component, the vertical distribution of oxygen in the atmosphere is very stable under varying atmospheric conditions. Thus, we can use the ratio of reflected radiance (or reflectance) at the top of atmosphere (TOA) of oxygen absorption and reference bands (i.e., R_{764} and R_{779} , R_{688} and R_{680}) to study the photon path length distribution and derive the cloud information. Also, compared to any specific EPIC oxygen absorption bands (i.e., R_{764} and R_{688}), the ratios of absorption to reference channels (i.e., R_{764}/R_{779} and R_{688}/R_{680}) are less impacted by the instrument calibration and other measurement error. This can be explained by the following reasons: First, the EPIC measurements at oxygen A and B absorption and reference bands share same sensor and optical system, when calculating the ratios of them, some preprocessing calibration errors can be reduced. Second, to calculate R_{764} and R_{688}, the ratio of lunar reflectance at neighboring channels (i.e.,$F(764,779)$ and $F(688,680)$) and the calibration factors of oxygen A and B reference bands (i.e., K_{779} and K_{680}) are used (Geogdzhayev and Marshak, 2018; Marshak et al., 2018). Therefore, the accuracy of R_{764} and R_{688} is determined by the stability of $F(764,779)$

4

143 and $F(688,680)$ and the accuracy of K_{779} and K_{680} together. But the accuracy of absorption to
144 reference ratios is only determined by the stability of $F(764,779)$ and $F(688,680)$.

145

2.2 Theory of CTP retrieval based on EPIC oxygen A- and B- band observation

147   In our study, we tried two methods to retrieve the CTP based on EPIC oxygen A-band and
148 B-band measurements: (1) Build a lookup table (LUT) for various atmospheric conditions and do
149 the retrieval by searching the LUT; (2) Develop an analytic transfer inverse model for EPIC
150 observations and calculate the related coefficients based on a series of simulated values, then use
151 this analytic transfer inverse model to retrieve the CTP. In this paper, we mainly focus on the
152 second method.

2.2.1 Method 1: LUT based approach

154   One commonly used method of retrieval for satellite observation is through the building
155 and usage of LUTs (Loyola et al., 2018, Gastellu-Etchegorry and Esteve, 2003). LUT based
156 approach can be fast because the most computationally expensive part of the inversion procedure
157 is completed before the retrieval itself. For DSCOVR EPIC observations, we can build LUTs by
158 simulating EPIC measurements under various atmospheric conditions, such as different surface
159 albedo, solar zenith and viewing angles, COD, CTP, and cloud pressure thickness. Comparing
160 the related simulated reflectance at the oxygen absorption and reference bands, we can obtain
161 two LUTs for reflectance ratios of absorption/reference at EPIC oxygen A-band and B-band
162 respectively, which can be used for the CTP retrieval. The detailed information of simulated
163 reflectance ratio of absorption/reference is stated in Section 2.3.3.

164   During the retrieval process, the EPIC measurements (e.g., reflectance at oxygen A and B
165 bands) with related solar zenith and viewing angles can be obtained from the EPIC level 1B data;
166 COD information (retrieved from other EPIC channels) can be obtained from EPIC level 2 data.
167 At the same time, we can get surface albedo from Global Ozone Monitoring Experiment 2
168 (GOME-2) Surface Lambertian-equivalent reflectivity (LER) data (Tilstra et al., 2017). At this
169 point the CTP and cloud pressure thickness are the only unknown variables. The cloud pressure
170 thickness or the cloud vertical distribution has substantial impact on the accuracy of the CTP
171 retrievals (Carbajal Henken et al., 2015; Fischer and Grassl, 1991; Rozanov and Kokhanovsky,
172 2004; Preusker and Lindstrot, 2009). In this study, the cloud pressure thickness is used as an
173 input parameter to retrieve the CTP. However, no related accurate cloud pressure thickness is
174 provided by other satellite sensors now. To constrain the error from the estimation of cloud
175 pressure thickness, we related it to the cloud optical thickness. It is reasonable because clouds
176 with higher optical thickness normally have higher values of pressure thickness. To explore the
177 correlation between cloud pressure thickness and cloud optical thickness, we use the related
178 cloud data from Modern-Era Retrospective analysis for Research and Applications Version 2
179 (MERRA-2, Gelaro et al., 2017), which is a NASA atmospheric reanalysis for the satellite era
180 using the Goddard Earth Observing System Model Version 5 (GEOS-5) with Atmospheric Data
181 Assimilation System (ADAS). Based on statistical analysis of one year's single-layer liquid
182 water clouds over an oceanic region (S23.20, W170.86, S2.11, W144.14) in 2017, we can get an
183 equation for cloud pressure thickness approximation, i.e., cloud pressure thickness (mb) = 2.5*

184 COD + 23. The derived correlation coefficients are dependent on the case region and time
185 selections. Due to the complexity of cloud vertical distribution, whatever the accuracy of the
186 correlation coefficients is, the estimation will certainly bring in error.

187 With an estimated cloud pressure thickness, a multi-variable LUT searching method can
188 then be used to interpolate and obtain the CTP. It is worth noting that the reflectance ratio of
189 absorption/reference can be seen as a function of surface albedo, solar zenith and viewing angles,
190 COD, CTP, and cloud pressure thickness. Some atmospheric variables will have a non-linear
191 effect on the reflectance ratio. For example, the reflectance ratio is more sensitive to the variation
192 of COD when COD is small. Overall, the reflectance ratio varies monotonically and smoothly
193 with these variables (shown in Figure 3). With a relatively high-resolution simulated table, we
194 can use a localized linear interpolation method to estimate the proper values. Multiple
195 interpolations are needed for this method to decrease the number of LUT dimensions, which will
196 cost more time than the analytic transfer inverse model method. The retrieval error of this
197 method is determined by the resolution of the LUT, i.e., the higher the resolution, the higher
198 retrieval accuracy. However, for multiple dimensional LUTs, the increase of resolution will
199 increase the table size exponentially, which will increase computational cost substantially for the
200 table building and inverse searching. Another possible method to increase the retrieval accuracy
201 is using different interpolation methods. For example, if the value of LUT varies non-linearly
202 with a variable, using high order interpolation method maybe better than using linear
203 interpolation method (Dannenberg, 1998).

204 **2.2.2 Method 2: Analytic transfer inverse model**

205 For a long time, various efforts have been devoted to the study of radiative transfer in the
206 atmosphere, including scattering, absorption, emission, and etc. (Chandrasekhar, 1960; Irvine
207 1964; Ivanov and Gutshabash 1974; van de Hulst, 1980, 2012; Ishimaru, 1999; Thomas and
208 Stamnes, 2002; Davis and Marshak, 2002; Kokhanovsky et al., 2003; Marshak and Davis, 2005;
209 Pandey et al., 2012; and etc.). In this study, we develop an analytic radiative transfer equation to
210 analyze the radiative transfer at oxygen A and B bands. Through solving the analytic equation,
211 we can retrieve the CTP information directly. The theory of CTP retrieval is similar for EPIC
212 oxygen A-band and B-band observation. Here we use oxygen A-band as an example to study the
213 radiative transfer model. For oxygen A-band, photon path length distribution is capable of
214 describing vital information related to a variety of cloud and atmospheric characteristics.

215
$$I_v(\mu, \varphi; \mu_0, \varphi_0) = I_0(\mu, \varphi; \mu_0, \varphi_0) \int_0^\infty p(l, \mu, \varphi; \mu_0, \varphi_0) e^{-\kappa_v l} dl \qquad (1)$$

216 Where, $p(l)$ is photon path length distribution, κ_v is the gaseous absorption coefficient at wave
217 number v, $\mu = cos(\theta), \mu_0 = cos(\theta_0)$, $(\theta, \varphi; \theta_0, \varphi_0)$ are zenith and azimuth angles for solar and
218 sensor view respectively, I_0 and I_v are incident solar radiation and sensor measured solar radiation,
219 respectively.

220 When clouds exist, the incident solar radiation is reflected to TOA in three primary ways.
221 First, incident solar radiation is reflected by cloud top layer directly as a result of single
222 scattering. Second, the incident solar radiation will penetrate into the cloud and be reflected back
223 to TOA through cloud top via multiple scattering. Third, the incident solar radiation will pass
224 through the cloud and arrive at the surface, after that it is reflected back into the cloud and finally

225 scattered back to TOA through the cloud top. Due to the position of the EPIC instrument and the
226 long distance between EPIC and Earth, we can consider that solar zenith angle and sensor view
227 angle are nearly reverse. At oxygen A-band, the reflected solar radiation will be reduced due to
228 oxygen absorption depending on photon path length distributions. Absorption is negligible in
229 oxygen A-band's reference band. Oxygen A-band and its reference band are also attenuated by
230 airmass and aerosol through Rayleigh scattering and aerosol extinction. In the standard
231 atmospheric model, the optical depth of Rayleigh scattering (τ_{Ray}) at oxygen A-band (B-band)
232 and its reference band is 0.026 (0.040) and 0.024 (0.042), respectively (Bodhaine et al., 1999).
233 The absolute difference of Rayleigh scattering optical depth ($\Delta\tau_{Ray} = \tau_{Ray}^{In-band} - \tau_{Ray}^{Ref}$) between
234 them is within 0.002. Compared to Rayleigh scattering, the difference of background aerosol
235 optical depth ($\Delta\tau_{Aer}$) between absorbing and reference bands is smaller, within 0.0005.
236 Therefore, the attenuations from Rayleigh scattering and aerosol extinction at EPIC oxygen
237 absorption and its reference band are close to each other. Thus, when we use the ratio of EPIC
238 measured reflectance at oxygen A-band and its reference band to derive the photon path length
239 distribution and retrieve cloud information such as CTP, the impact of Rayleigh scattering and
240 aerosol extinction can be simplified in the analytic transfer inverse model.

241   To simplify the analytic transfer inverse model for EPIC observations, we made a series
242 of assumptions, e.g., isotropic component, a plane-parallel homogenous cloud assumption with
243 quasi-Lambertian reflecting surfaces. These assumptions have been widely used in radiative
244 transfer calculation for cloud studies. In this model, μ and μ_0 are the same as in Eq. (1), φ is the
245 relative azimuth angle between Sun and satellite sensors; A_{surf} is the surface albedo; τ_{O2}^{Top}, τ_{O2}^{Base},
246 and $\tau_{O2}^{Surface}$ are oxygen A-band absorption optical depth from TOA to cloud top layer, cloud
247 bottom layer, and surface, respectively; $\Delta\tau_{O2}^{Above-Cld}$, $\Delta\tau_{O2}^{In-Cld}$ and $\Delta\tau_{O2}^{Below-Cld}$ are layered
248 oxygen A-band absorption optical depth above cloud, in cloud, and below-cloud, respectively;
249 functions f mean their contribution to the ratio of measured reflectance at oxygen A-band (R_A)
250 and refrence band (R_f). The detailed analysis of EPIC analytic transfer inverse model is shown
251 as follows:

252 (1) **Above Cloud**: the reflected solar radiation is determined by the oxygen absorption optical
253 depth above the cloud and air mass directly.

$$f\left(\Delta\tau_{O2}^{Above-Cld}, \mu_0, \mu, \varphi\right) = f\left(\Delta\tau_{O2}^{Above-Cld}\right)f\left(\mu_0, \mu, \varphi\right)$$

$$= a_0 \tau_{O2}^{Top}\left(\frac{1}{\mu} + \frac{1}{\mu_0}\right) \tag{2}$$

256 Here, a_0 is a weight coefficient.

257 (2) **Within Cloud**: the reflected solar radiation is not only determined by oxygen absorption
258 optical depth above cloud and in-cloud, but also by penetration related factors, e.g., COD. Due to
259 photon penetration, oxygen parameter τ_{O2}^{Top} influences the enhanced path length absorption:

$$\Delta\tau_{O2}^{In-Cld} = \tau_{O2}^{Base} - \tau_{O2}^{Top} \tag{3}$$

261 Equivalence theorem (Irvine, 1964; Ivanov and Gutshabash, 1974; van de Hulst 1980) is used to
262 separate absorption from scattering:

7

263 $$f(\tau_{O2}^{Top}, \Delta\tau_{O2}^{In-Cld}, \mu_0, \mu, \varphi) = f(\tau_{O2}^{Top}, \Delta\tau_{O2}^{In-Cloud})f(\mu_0, \mu, \varphi)$$

264 $$= f(\tau_{O2}^{Top})f_1(\mu_0, \mu, \varphi) + f(\Delta\tau_{O2}^{In-Cloud})f_2(\mu_0, \mu, \varphi) \tag{4}$$

265 $f(\tau_{O2}^{Top})$ is determined by two absorption dependences: strong ($\sim \sqrt{\tau_{O2}^{Top}}$) and weak ($\sim \tau_{O2}^{Top}$).

266 $$f(\tau_{O2}^{Top}) = a_1 \sqrt{\tau_{O2}^{Top}} + b_1(\tau_{O2}^{Top}) \tag{5}$$

267 Based on asymptotic approximation (*Kokhanovsky et al., 2003; Pandey et al., 2012*), the
268 reflection of a cloud without considering below cloud interaction is given by Eq. (6):

269 $$R(\tau, \mu, \mu_0, T) = R_0^\infty(\tau, \mu, \mu_0) - TK(\mu)K(\mu_0)$$

270 $$= R_0^\infty(\tau, f_1(\mu, \mu_0)) - Tf_2(\mu, \mu_0) \tag{6}$$

271 Here, R_0^∞ is the reflectance of a semi-infinite cloud, $K(\mu)$ is the escape function of μ, T is global
272 transmittance of a cloud. T can be estimated by Eq. (7), with the cloud optical thickness τ_{cld}, the
273 asymmetry parameter , and a numerical constant $\alpha = 1.07$.

274 $$T = \frac{1}{0.75\tau_{cld}(1-g)+\alpha} \tag{7}$$

275 f_1 and f_2 functions have a quadratic form as follows:

276 $$f_{i-1} = a_i T + b_i(\mu + \mu_0) + c_i T(\mu + \mu_0) + d_i \mu\mu_0, i = 2,3 \tag{8}$$

277 Combining Eqs. (4), (5) and (8), we can get the Eq. (9):

278 $$f(\tau_{O2}^{Top}, \Delta t_{O2}^{Cld}, \mu_0, \mu, \varphi) = \left(a_1\sqrt{\tau_{O2}^{Top}} + b_1(\tau_{O2}^{Top})\right)\left(a_2 T + b_2(\mu + \mu_0) + c_2 T(\mu + \mu_0) + d_2\mu\mu_0\right)$$

279 $$+ \Delta\tau_{O2}^{In-Cloud}\left(a_3 T + b_3(\mu + \mu_0) + c_3 T(\mu + \mu_0) + d_3\mu\mu_0\right) \tag{9}$$

280

281 (3) **Below Cloud**: The equivalence theorem used for below cloud is similar to within cloud
282 (Kokhanovsky et al., 2003; Pandey et al., 2012).

283 $$f(\Delta\tau_{O2}^{Below-Cld}, \mu_0, \mu, \varphi) = T\,\tau_{O2}^{Surface}\frac{A_{Surf}}{1+(e_4 * T + f_4)*A_{Surf}}$$

284 $$* (a_4 T + b_4(\mu + \mu_0) + c_4 T(\mu + \mu_0) + d_4\mu\mu_0) \tag{10}$$

285

286 Combining Eqs. (2), (9) and (10), we can get the total EPIC analytic transfer equation as
287 follows

288 $$-log\left(\frac{R_A}{R_f}\right) = f(\Delta\tau_{O2}^{Above-Cld}, \mu_0, \mu, \varphi) + f(\tau_{O2}^{Top}, \Delta\tau_{O2}^{Cld}, \mu_0, \mu, \varphi) +$$

289 $$f(\Delta\tau_{O2}^{Below-Cld}, \mu_0, \mu, \varphi) + \Delta\tau_{BG}\left(\frac{1}{\mu}+\frac{1}{\mu_0}\right) \tag{11}$$

290 In Eq. (11), $\Delta\tau_{BG}$ represents the sum of optical depth difference of background extinction (i.e.,
291 Rayleigh scattering $\Delta\tau_{Ray}$, aerosol extinction $\Delta\tau_{Aer}$, and O3 $\Delta\tau_{O3}$) between oxygen in-band and
292 reference band, as shown in Eq. (12).

293
$$\Delta\tau_{BG} = \Delta\tau_{Ray} + \Delta\tau_{Aer} + \Delta\tau_{O3} \qquad (12)$$

294 As stated in the previous subsection, in the standard atmospheric model with background aerosol
295 loading, ($\Delta\tau_{Ray}$, $\Delta\tau_{Aer}$, $\Delta\tau_{O3}$) is approximately (0.002, 0.0005, -0.0005) and (-0.002, -0.0005, -
296 0.002) respectively at oxygen A and B bands, thus $\Delta\tau_{BG}$ is approximately 0.002 and -0.0045
297 respectively at these two bands.

298 In this total analytic equation, there are 17 coefficients ($a_0, a_1, b_1, a_2, \dots d_4, e_4, f_4$), which
299 can be calculated through nonlinear regression algorithm according to a series of simulated
300 values for different atmospheric conditions. Based on Eq. (11), we can finally obtain a quadratic

301 equation, $\mathbf{A}\sqrt{\tau_{O2}^{Top}}^2 + \mathbf{B}\sqrt{\tau_{O2}^{Top}} + \mathbf{C} = \mathbf{0}$, where the parameters A, B and C can be derived from
302 Eq. (11) directly, as shown in Eq. (13).

303
$$A = a_0\left(\frac{1}{\mu} + \frac{1}{\mu_0}\right) + b_1\left(a_2 T + b_2(\mu + \mu_0) + c_2 T(\mu + \mu_0) + d_2\mu\mu_0\right) \qquad (13.1)$$

304
$$B = a_1\left(a_2 T + b_2(\mu + \mu_0) + c_2 T(\mu + \mu_0) + d_2\mu\mu_0\right) \qquad (13.2)$$

305
$$C = -log\left(\frac{R_A}{R_f}\right) - \Delta\tau_{BG}\left(\frac{1}{\mu} + \frac{1}{\mu_0}\right) - \Delta\tau_{O2}^{In-Cloud}\left(a_3 T + b_3(\mu + \mu_0) + c_3 T(\mu + \mu_0) + d_3\mu\mu_0\right)$$

306
$$-T\,\tau_{O2}^{Surface}\frac{A_{Surf}}{1+(e_4*T+f_4)*A_{Surf}}\left(a_4 T + b_4(\mu + \mu_0) + c_4 T(\mu + \mu_0) + d_4\mu\mu_0\right) \quad (13.3)$$

307 When these parameters (i.e., A, B and C) are obtained from EPIC observation data and
308 other data source, we can easily solve the quadratic equation to retrieve cloud top O2 absorption
309 depth, and then CTP.

310 2.3 Detailed retrieval algorithm

311 As previously stated, in method 2, the analytic EPIC equation (i.e., Eq. (11)) is key for the
312 CTP retrieval. To derive the coefficients of Eq. (11), a series of model simulations for various
313 atmospheric conditions are needed. Thus, developing a radiative transfer model to simulate the
314 EPIC measurements at A- and B-bands and their reference bands is the first thing we need to
315 complete.

316 2.3.1 Oxygen A- and B-band absorption coefficients calculation

317 To simulate the EPIC measurements, one of the most important steps is calculating
318 oxygen absorption coefficients at oxygen A-band and B-band. In this step, the HITRAN 2016
319 database is used to provide the absorption parameters, and the LBLRTM package is used to
320 calculate oxygen absorption coefficients layer by layer. In our algorithm, the whole Earth
321 atmosphere is divided by 63 layers.

322 Since oxygen absorption coefficients are pressure (or pressure-squared) and temperature
323 dependent, and the line shapes (k_i) of oxygen A- and B-bands are well fitted as Lorentzian in the
324 lower atmosphere, the relationship can be written as follows:

325
$$k_i = \frac{S_i}{\pi}\frac{\alpha_i}{(v-v_i)^2+\alpha_i^2} \qquad (14)$$

$$\alpha_i = \alpha_i^0 \frac{P}{P_0} \left(\frac{T_0}{T}\right)^{\frac{1}{2}}, \ S_i = S(T_0)\frac{T_0}{T} \exp\left[1.439E\left(\frac{1}{T_0} - \frac{1}{T}\right)\right] \qquad (15)$$

Where S_i is the line intensity, v_i and α_i are the line center wave number and half width, respectively; P_0 and T_0 are standard atmospheric pressure and temperature, respectively.

In the simulation of EPIC measurements, the atmospheric layer at a given layer-average pressure can have drastically different temperature depending on the atmospheric profile in use. To ensure the accuracy of simulation, we need to use the LBLRTM package to calculate oxygen absorption coefficients for each pressure/temperature profile, which is a time-consuming process. Our goal has been to find a simple and fast method to calculate oxygen absorption coefficients for different atmospheric profiles. Based on the study of Chou and Kouvaris (1986), Min et al. (2014) proposed a fast method to calculate oxygen absorption optical depth for any given atmosphere by using a polynomial fitting function, as shown in Eq. 16.

$$\ln(A_{vLM}) = [a_0(v, P) + a_1(v, P) \times (T_{LM} - T_{mL}) + a_2(v, P) \times (T_{LM} - T_{mL})^2] \times \rho_{O_2} \ (16)$$

Where A_{vLM} is optical depths for layer L, spectral point v, and atmosphere model M; ρ_{O_2} is molecular column density ($\frac{molecules}{cm^2} \times 10^{-23}$); T_{LM} is the average temperature for layer L for a given atmosphere; and T_{mL} is average temperature over all six typical geographic-seasonal model atmospheres (M1 to M6, i.e., tropical model, mid-latitude summer model, mid-latitude winter model, subarctic summer model, subarctic winter model, and the U.S. Standard (1976) model) for layer L. To derive the coefficients a_0, a_1, and a_2, we first calculated oxygen optical depth coefficients for all typical atmospheres (M1 to M6) by using LBLRTM package, and then selected three of them (e.g., M1, M5, and M6) to calculate the polynomial fitting coefficients. This method has been successfully used by Min et al. (2014) to simulate the high resolution oxygen A-band measurements.

2.3.2 Fast radiative transfer model for simulating high-resolution oxygen A- and B-bands

At oxygen A and B absorption bands, there are lots of absorption lines, therefore we cannot simply calculate narrowband mean optical depth and then calculate the radiation for various atmospheric conditions when simulating EPIC narrowband measurements. The correct way is described as follows: firstly, simulate the solar radiation spectrum $S(k(\lambda))$ under specific atmospheric conditions, then integrate the spectrum with EPIC narrowband filter $R(k(\lambda))$ to obtain simulated narrowband measurements (Eq. (17)).

$$R(\lambda) = \int S(k(\lambda))R(k(\lambda))d\lambda \neq R(\overline{k(\lambda)}) \qquad (17)$$

With the high spectrum resolution oxygen absorption coefficient data, we can simulate the high resolution upward diffuse oxygen A-band or B-band spectrum through DISORT code (Stamnes et al., 1988) for any given atmospheric condition, which has various surface albedo, SZA, COD, CTH (CTP), and cloud geometric (pressure) thickness. However, due to the high spectrum resolution, it is very time-consuming when performing line by line (LBL) calculations. Thus, developing a fast radiative transfer model for simulating high resolution oxygen A-band and B-band spectrum is necessary.

In this project, the double-k approach is used to develop a fast radiative transfer model for oxygen A-band and B-band respectively. [Min and Harrison 2004; Duan et al, 2005] proposed a

365 fast radiative transfer model. In their approach, the radiation from absorption and scattering
366 processes of cloud and aerosol are split into the single- and multiple-scattering components: The
367 single scattering component is computed line-by-line (LBL), while multiple scattering (second
368 order and higher) radiance is approximated.

369 $$I = I^{ss}(\lambda) + I^{ms}(\lambda)$$

370 $$\approx I^{ss}[Z^h(p,T), P^h, \lambda] + I^{ms}[Z^h(p,T), P^h, \lambda]$$

371 $$\approx I^{ss}[Z^h(p,T), P^h, \lambda] + I^{ms}[Z^l(p,T), P^l, \lambda]$$

372 $$\approx I^{ss}[Z^h(p,T), P^h, \lambda] + I^{ms}\{F[Z^l(p,T), P^l, k(\lambda_i)]\} \qquad (18)$$

373 Eq. (18) is from Eq. (1) in Duan et al. (2005): *ss* and *ms* mean single and multiple scattering,
374 respectively. Z is the optical properties of the atmosphere as a function of pressure *p* and
375 temperature *T*, with P being the phase function of that layer. *h* and *l* represent higher and lower
376 number of layers and streams, respectively. F is the transform function between wave number
377 space and k space, defined from a finite set of $k(\lambda_i)$.

378 The application of Double-*k* approach in oxygen A-band has been presented in detail in
379 Duan et al. 2005. Here we take oxygen B-band as an example. The detailed fast radiative transfer
380 model for simulating high-resolution oxygen B-band is as follows: The first order scattering
381 radiance is calculated accurately by using a higher number of layers and streams for all required
382 wavenumber grid points. The multiple-scattering component is extrapolated and/or interpolated
383 from a finite set of calculations in the space of two integrated gaseous absorption optical depths
384 to the wavenumber grids: a double-*k* approach. The double-*k* approach substantially reduces the
385 error due to the uncorrelated nature of overlapping absorption lines. More importantly, these
386 finite multiple-scattering radiances at specific *k* values are computed with a reduced number of
387 layers and/or streams in the forward radiative transfer model. To simulate an oxygen B-band
388 spectrum with high accuracy, 33 *k* values and 99 calculations of radiative transfer are chosen in
389 our program. This results in around a hundred-fold time reduction with respect to the standard
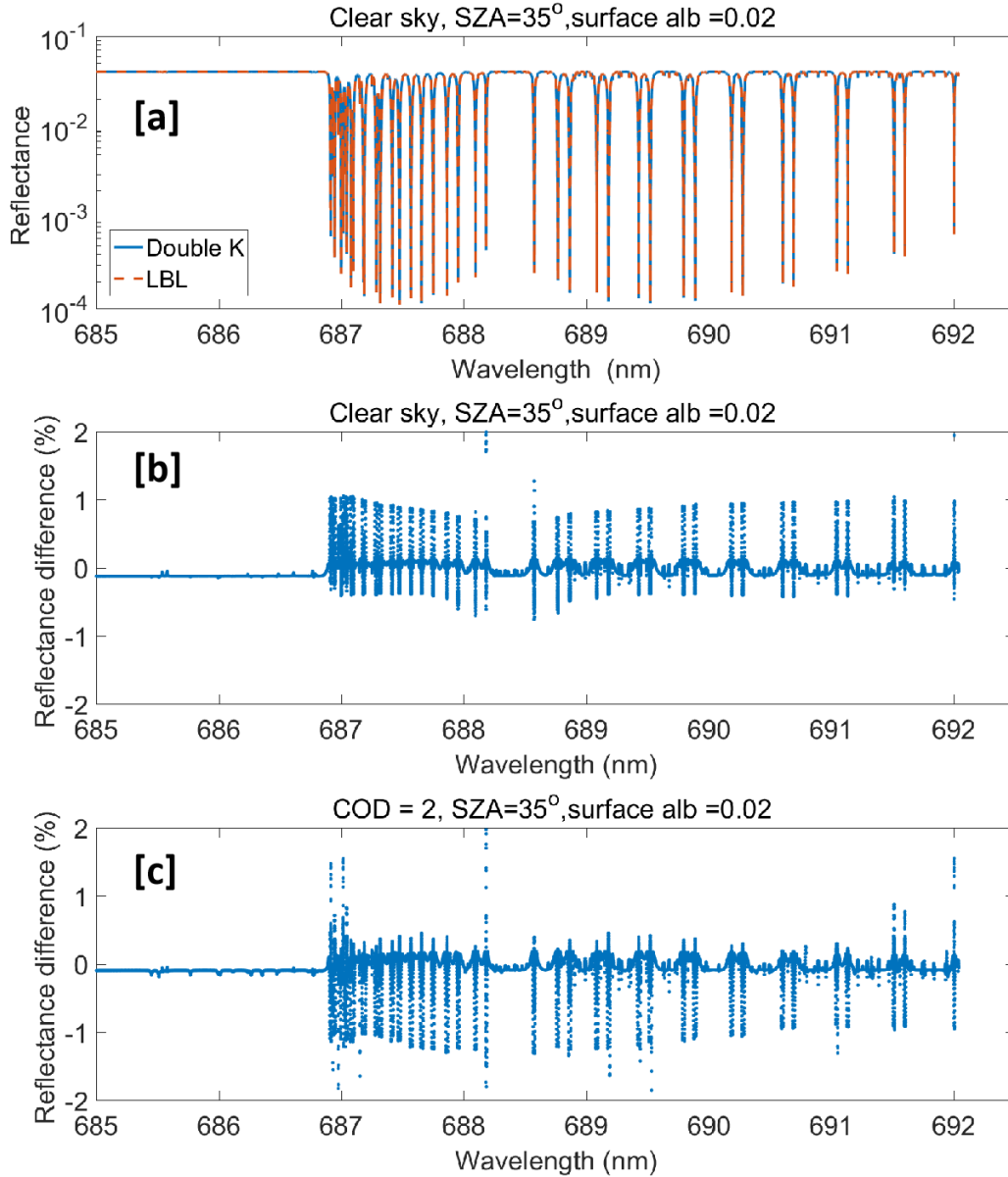390 forward radiative transfer calculation.

Figure 2. [a] High resolution reflectance at EPIC O2 B-Band simulated by fast radiative model (double-k) and benchmark (LBL); Difference between simulated reflectance by double-k and LBL for a clear sky case [b] and a thin liquid water cloud case with COD=2 [c]. Here SZA and view angle =35°, surface albedo = 0.02, aerosol optical depth = 0.08, and reflectance difference (%) = 100*((double-k) – LBL)/LBL.

As shown in Figure 2, under clear sky and thin liquid water cloud situations, the simulated high resolution upward diffuse oxygen B-band spectra from LBL calculation and double-k approach are compared. The spectrum difference between LBL calculation and double-k approach is very small (Figure 2a). Under both situations, most of the relative difference between these two methods are under 0.5%. The obvious relative difference (>1%) occurs only in the wavelength range with high absorption optical depth, which has little contribution to the integrated solar radiation. Therefore, for the simulated narrowband measurements at EPIC

404 oxygen B-band, the relative difference between LBL and double-k approach is much smaller
405 than that of the high resolution spectrum, which is less than 0.1% for clear day. Compared to
406 clear sky situation, the relative difference for cloud situations can be bigger. As shown in Table
407 1, the relative difference is -0.06% and -0.32% for typical high level optical thin cloud and low-
408 level thick cloud situations, respectively. The comparison of simulated narrowband measurement
409 at EPIC oxygen A-band channel (764 nm) is also shown in Table 1, the relative differences
410 between LBL and double-k approach are -0.06%, 0.21% and 0.23% for clear day, high level thin
411 cloud and low level thick cloud cases, respectively. In general, the accuracy of double-k
412 approach for both oxygen A and B absorption bands is high.

413 **Table 1.** Comparison of simulated narrowband measurement at EPIC A- and B-Band channels

Case (SZA=35, surface albedo =0.02)		Line by Line	Double k	Relative Difference
Clear Day	688 nm	0.026963	0.026985	+0.08%
	764 nm	0.013979	0.013970	-0.06%
Thin cloud (COD=2, 8.3-8.5 km, liquid)	688 nm	0.098444	0.098131	-0.32%
	764 nm	0.071359	0.071507	+0.21%
Thick cloud (COD=16, 1.5-2.9 km, liquid)	688 nm	0.396354	0.396117	-0.06%
	764 nm	0.233937	0.234485	+0.23%

414

415 **2.3.3 Simulation of oxygen A- and B-bands for different atmospheric conditions**

416   Using the EPIC measurement simulation package, we made a series of simulations with
417 different settings for surface albedo, solar zenith angle, COD, CTH (CTP), and cloud geometric
418 (pressure) thickness (or cloud bottom height). The results of these simulations consist of a data
419 table, which can be used not only to calculate the coefficients for the analytic equation, but also
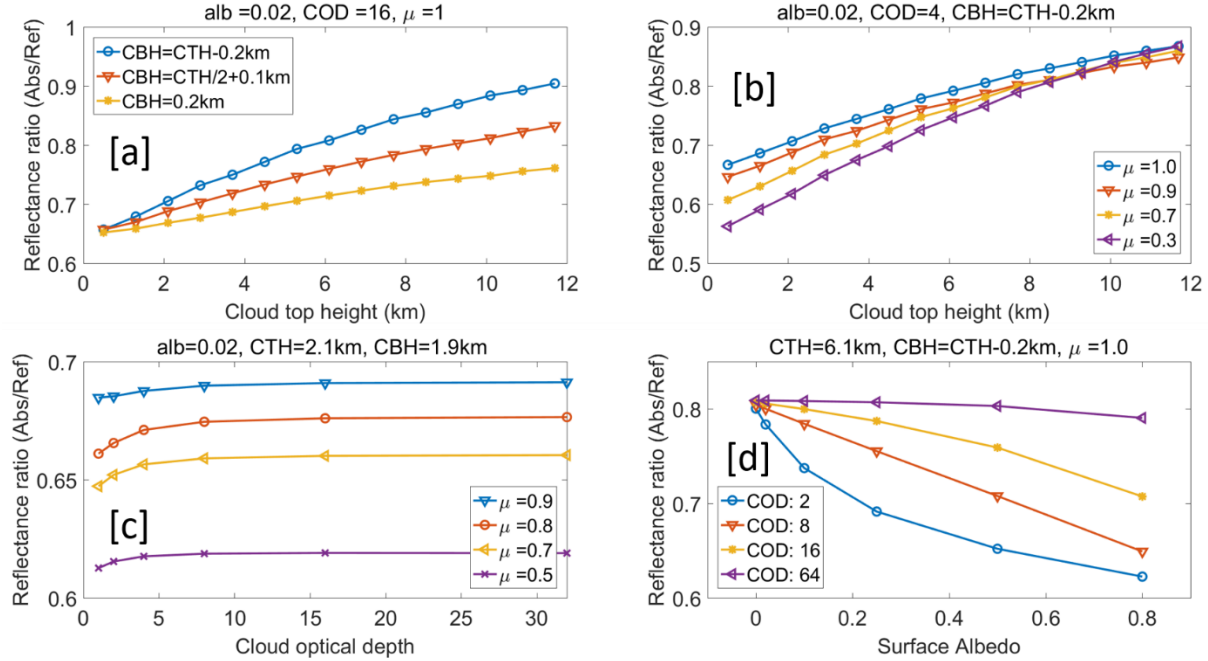420 to study the sensitivity of every variable.

421

Figure 3. Ratio of simulated reflectance measurements for EPIC B-band to B-band reference with different surface albedo (alb), COD, μ (cosine of solar zenith angle), cloud top height (CTH) and cloud bottom height (CBH).

According to the previous theory study, the ratio of reflectance radiance (i.e., absorption to the reference) at TOA is determined by the photon path length distribution at oxygen A/B bands: the larger the mean photon path length, the stronger the absorption, and the smaller the reflectance ratio. To make the figures easy to view and understand, we use cloud top and bottom geometric height to represent CTP and thickness information in Figure 3. As shown in Figure 3a, the ratio of upward diffuse radiance at oxygen B-band and its reference band is sensitive to the cloud top height (pressure). The higher the CTH, the larger the ratio. At the same time, this ratio is affected by the cloud bottom height (or cloud geometric thickness) when the other cloud parameters are fixed, the lower the cloud bottom (or the larger the cloud geometric thickness), the smaller the ratio. It is consistent with the theory analysis: (1) the higher the CTH, the shorter the mean photon path length, and the weaker the absorption; (2) when the COD is given, larger cloud geometric thickness means smaller cloud density, then the sunlight can penetrate deeper into the cloud, which results in a longer mean photon path length. In Figure 3b, for clouds with given CTH, COD and geometric thickness, the ratio decreases with the solar and view angles. This can be understood as: the larger the solar and view angles, the longer the mean photon pathlength, and the stronger the absorption. In Figure 3c, for clouds with given CTH and geometric thickness, when the COD is small (e.g., COD <5), the reflectance ratio increases with COD. However, when COD is larger than 16, the effect of COD is small. This is because the larger the COD, the shallower the sunlight penetration, and the shorter the mean photon pathlength. In Figure 3d, for clouds with given COD, CTP, and geometric thickness, the ratio decreases with surface albedo. The smaller the COD, the stronger the impact of the surface albedo. This is because the thick cloud prevents the incident sunlight from passing through it to reach the surface, and also prevents the reflected light from going back to the TOA.
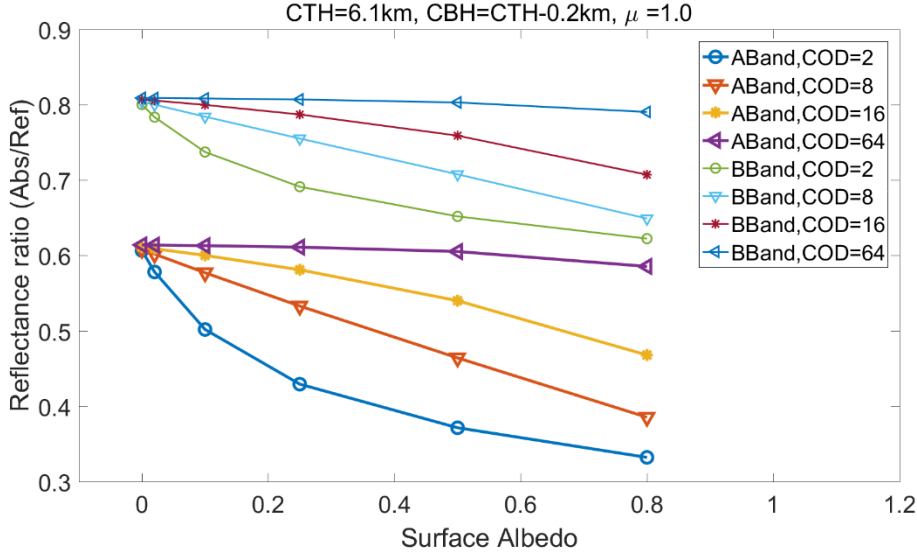
Figure 4. Ratio of simulated reflectance measurements for EPIC A and B absorption band to reference band with different surface albedo.

For oxygen A-band, the ratio of upward diffuse at absorption and reference bands shows similar characteristics as for oxygen B-band. Compared to oxygen B-band, under the same atmospheric conditions, the oxygen absorption at A-band is stronger, and the ratio of A-band to its reference band has smaller values (shown in Figure 4). As stated previously, for land area that covered with plants, the surface albedo may change substantially from oxygen B-band to A-band due to the presence of the red edge. Therefore, accurate spectral data of surface albedo for CTP retrieval is vitally important, especially for optically thin clouds.

3. Application and validation of the CTP retrieval method

3.1 Case studies of CTP retrieval

The dataset of DSCOVR EPIC measurements at GMT 00:17:51 on July 25, 2016 is used for the case studies. The reflectance at oxygen A and B bands with related solar zenith and viewing angles are obtained from the EPIC level 1B data; COD information (retrieved from other EPIC channels) is obtained from EPIC level 2 data. The surface albedo data is obtained from Global Ozone Monitoring Experiment 2 (GOME-2) Surface Lambertian-equivalent reflectivity (LER) data. The detailed information of dataset is shown in the acknowledgements and dataset. To reduce the impact of the Earth surface, we selected the region located in spatial range of (S75° to N85°, W177° to W175°) for case studies, which is mainly covered by ocean. To constrain the influence of surface albedo and broken clouds, only pixels with total cloud cover (i.e., EPIC Cloud mask = 4), surface albedo less than 0.05, and liquid assumed COD larger than 3 are considered. In the selected region, around 10000 pixels are finally chosen for case studies.

In our retrieval algorithm, we have two kinds of retrieval results: baseline CTP and retrieved CTP. The baseline CTP is used as a reference for the retrieved CTP. It is similar to the effective CTP in Yang et al., (2019), which does not consider cloud penetration. The retrieved CTP is calculated by the analytic equation, which considers the in-cloud and below-cloud interaction.

15

During the baseline CTP calculation, the impact of penetration in-cloud is ignored, and the incident light that reached cloud top is assumed reflected back directly. As shown in Eq. (19), the baseline absorption optical depth τ_{base} is derived from the ratio of upward diffuse at absorption bands and their reference bands directly. According to the model calculated oxygen A and B bands absorption optical depth profile at the specific solar zenith angle, the baseline CTP can be derived directly.

$$\tau_{base} = \log\left(-\frac{R_{abs}}{R_{ref}}\right) / \left(\frac{1}{\cos(\theta_{sza})} + \frac{1}{\cos(\theta_{view})}\right) \tag{19}$$

As shown in Figure 5, the baseline CTP value at A-band is slightly higher than the effective CTP from NASA ASDC L2 data. But the baseline CTP value at B-band is substantially higher than the effective CTP from NASA ASDC L2 data. For both A-band and B-band, the difference between baseline CTP and effective CTP increases with the CTP. For low-level clouds, the mean differences of them are up to 60 mb and 100 mb at A-band and B-band, respectively. The difference may be mainly from the calculation of oxygen A and B bands absorption coefficients or the absorption optical depth profile.
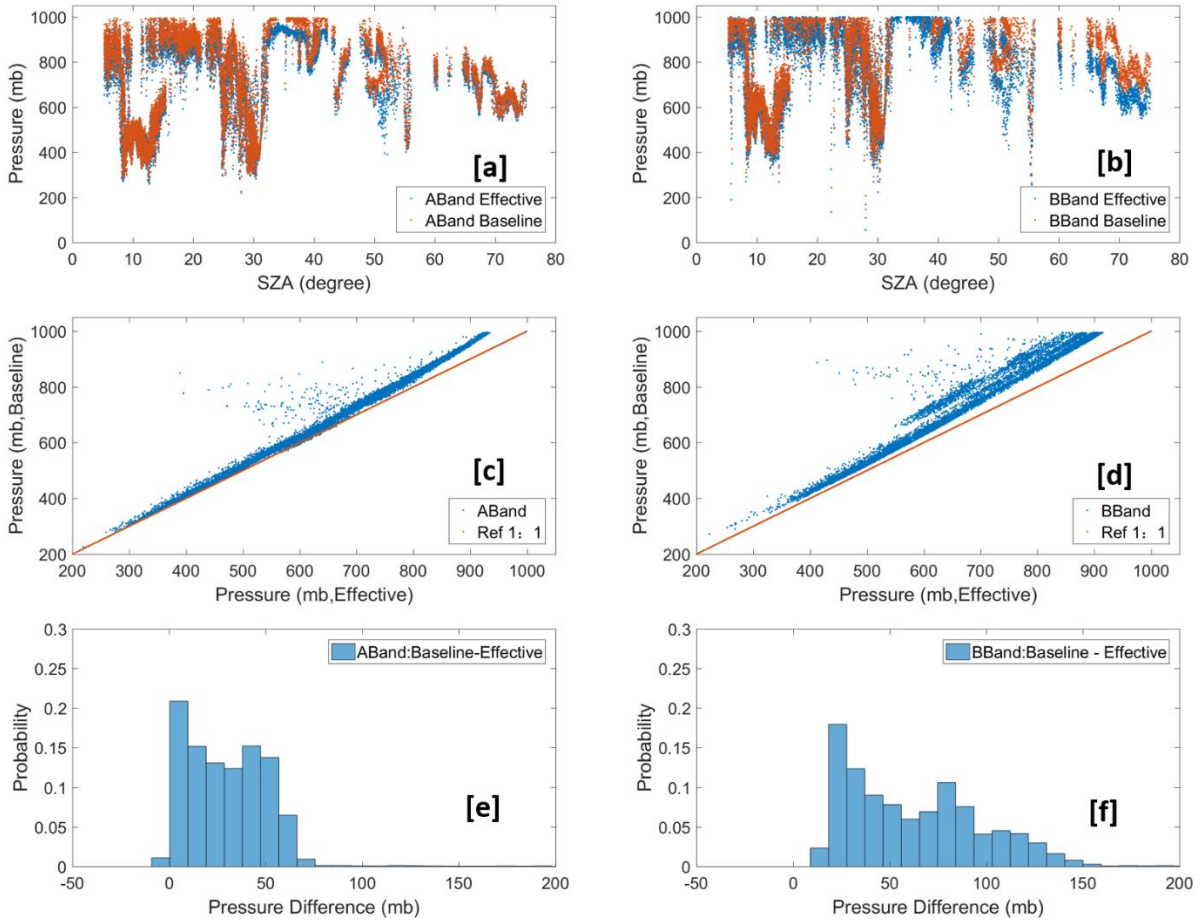

Figure 5. The comparison of effective CTP (reference from NASA ASDC data) and baseline values from our retrieval algorithm for EPIC A and B bands.

16

495   Based on the simulated reflectance ratio under different atmospheric conditions, we can
496   calculate the coefficients for the analytic radiative transfer equations by using a nonlinear fitting
497   algorithm. The coefficients for different SZA's are calculated individually to reduce the fitting
498   error. Based on the calculated coefficients, we can retrieve the CTP with DISCOVR EPIC
499   observation data at oxygen A and B bands.

500   During the CTP retrieval, with the exception of the previously mentioned analytic
501   equation coefficients, we can get the surface albedo data from GOME, obtain reflectance data,
502   solar zenith and view angles, COD, etc. from the NASA ASDC data file. Another very important
503   step in the retrieval processing is the acquisition of cloud pressure thickness data, which has a
504   substantial impact on the retrieval results. We currently use a statistical approach (i.e., cloud
505   pressure thickness (mb) = 2.5* COD +23) to estimate the cloud pressure thickness based on
506   COD. As shown in Figure 6a-6d, the retrieved CTP when considering cloud penetration is
507   smaller than baseline CTP. For this case, the mean difference between baseline CTP and
508   retrieved CTP for oxygen A-band and B-bands are around 57 mb and 85 mb, respectively, which
509   is consistent with theoretical expectations. For clouds with a given CTP, the mean photon path
510   length will increase substantially when considering cloud penetration. A decrease in retrieved
511   CTP will result in order to match the measurement ratio of absorption to reference. Compared to
512   the O2 A-band, both baseline CTP and retrieved CTP for the O2 B-band are larger (Figure 6e-
513   6h). This is because the absorption of solar radiation in the O2 B-band is weaker than that of the
514   O2 A-band, and the incident light at oxygen B-band can penetrate deeper into the cloud,
515   allowing more light to pass through. The difference in retrieved CTP between B band and A
516   band (approx. 93 mb with standard deviation of 83 mb) is generally reduced in comparison to
517   baseline B band and A band (approx. 114 mb with standard deviation of 73 mb). This indicates,
518   as expected, more photon penetration correction for B-band than A-band.
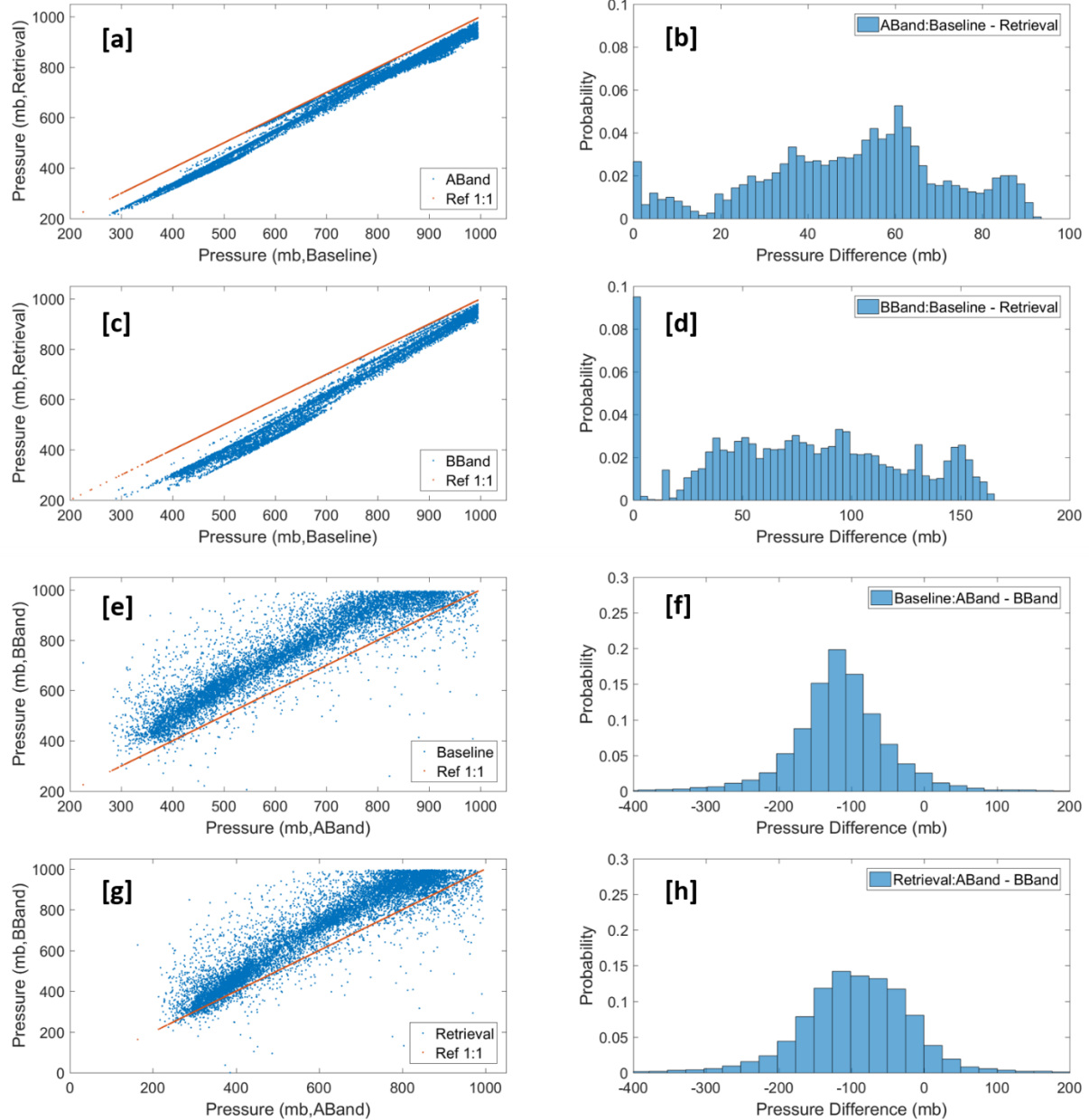
519

Figure 6. a-d) The comparison of retrieved CTP and baseline values for EPIC A and B bands; (e-f) the comparison of retrieved CTP and baseline values between EPIC A- and B- bands.

We also used the LUT based method to do the retrieval for the same observation data, because both methods share the same EPIC simulation package and the same simulated data table, the results of which are similar.

3.2 Validation of the retrieval method

To validate the analytic transfer inverse model method for CTP retrieval, we used another independent measurement of CTP, i.e., cloud layer top pressure from Cloud-Aerosol Lidar and Infrared Pathfinder Satellite Observations (CALIPSO, Vaughan et al., 2014) as a reference. For

18

531   the previously stated case, i.e., DSCOVR EPIC measurements at GMT 00:17:51 on July 25,
532   2016, we used the cloud layer data from CALIPSO IIR Version 4.2 Level 2 product with 5 km
533   resolution at GMT 00:01:47 on July 25, 2016 as its reference to do validation. To constrain the
534   error from spatial differences between different satellite measurements, we only chose the pixels
535   of EPIC and CALIPSO measurements with a spatial distance of within 0.1° (degree of latitude or
536   longitude) to make comparisons. For the EPIC measurements, the same as previously stated,
537   only pixels with total cloud cover (i.e., EPIC Cloud mask = 4), surface albedo less than 0.05, and
538   liquid assumed COD larger than 3 are considered. As shown in Figure 7a, there are a series of
539   pixels (around 400 cases) from EPIC and CALISPO measurements can be used for the validation
540   analysis. For the convenience of reading, we perform the analyses by using the case number as x
541   axis. Figure 7b shows the comparisons of cloud layer top pressure from CALIPSO and different
542   CTPs (i.e., effective CTP, baseline CTP, and retrieved CTP) from EPIC measurements. Figure
543   7c shows the cloud layer number measured by CALIPSO. According to Figures 7b and 7c, we
544   can get some results: under single layer cloud situations, the CTPs derived from EPIC
545   measurements are close to the CTP from CALISPO; under multi-layer cloud situations, the CTP
546   derived from EPIC measurements are larger than the CTP from CALISPO. Figure 7d shows the
547   expanded view of the Figure 7b for some cases under single layer cloud situations. For these
548   single layer cloud cases (with case number 46 ~ 156), the mean values of CTP of CALIPSO,
549   EPIC effective, EPIC baseline and EPIC retrieval are 846, 834, 866 and 850 mb, respectively.
550   Compared to the CTP from CALIPSO measurements , the EPIC effective and baseline CTPs are
551   12 mb smaller or 20 mb larger, respectively; the EPIC retrieval with consideration of photon
552   penetration is only 4 mb larger. This shows that our method for the CTP retrieval is valid and
553   accurate under single layer cloud situations with COD > 3 and low surface albedo. Under multi-
554   level cloud situations, the high-level clouds are often thin clouds, which can be detected by
555   CALIPSO but hard to derive by our retrieval method. It is because the EPIC retrieved CTP
556   mainly shows the pressure of cloud layer that reflects the major part of incident sun light.
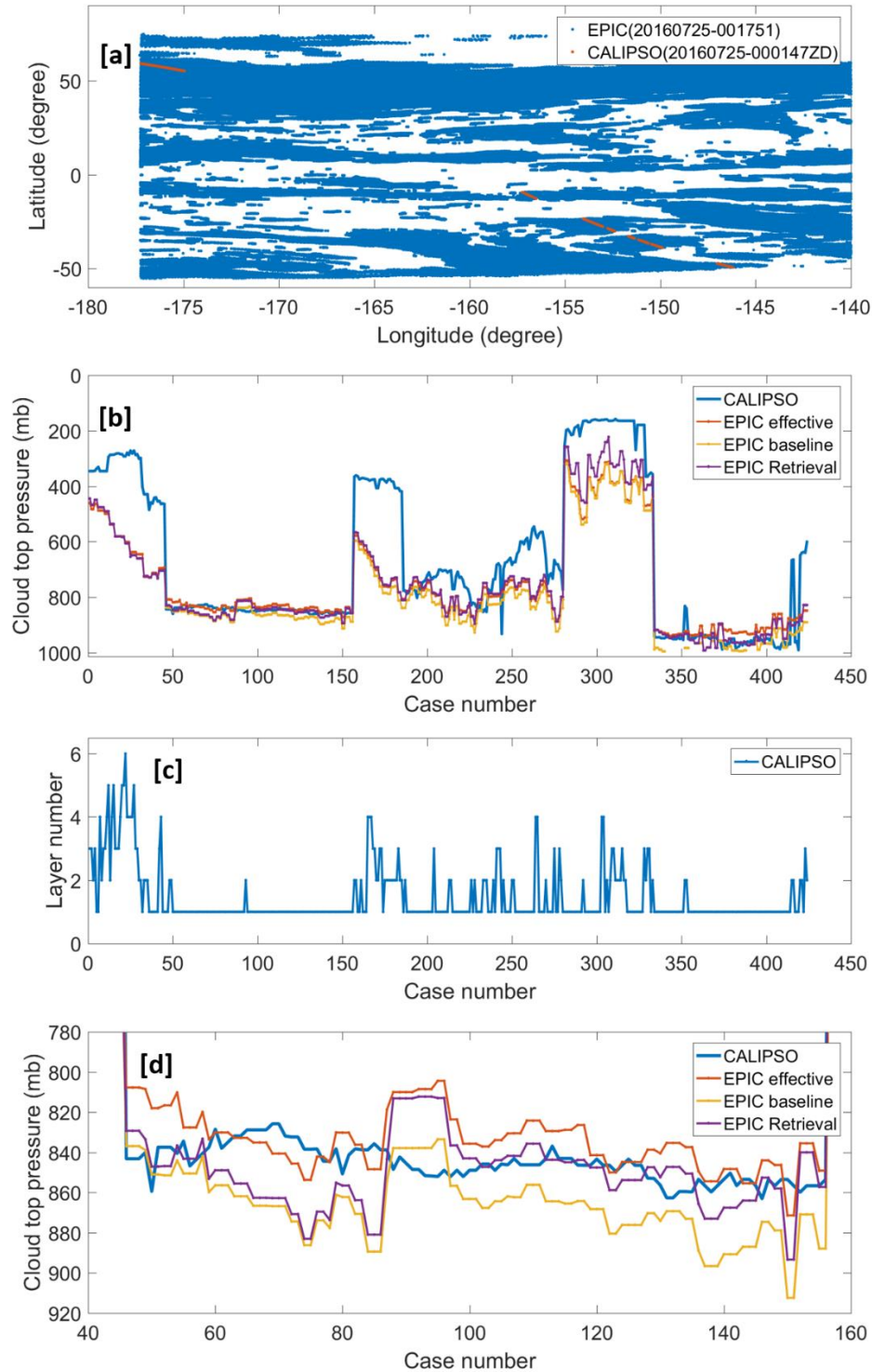
557

558

Figure 7. (a) The geolocation match of EPIC measurement at GMT 00:17:51 and CALISPO
measurement at GMT 00:01:47 on July 25, 2016; (b) the comparisons of cloud layer top pressure
from CALIPSO measurements and the CTPs derived from EPIC measurements; (c) the cloud
layer number from CALIPSO measurements; and (d) the expanded view of (b) for some cases
under single layer cloud situations.

564

3.3 Retrieval of global observation

We applied our retrieval algorithm on the global DISCOVR EPIC measurement data at oxygen A and B bands. During the retrieval, only pixels with total cloud cover (i.e., cloud mask index of 4), surface albedo < 0.25, and COD >= 3 are considered. To make the pictures easy to visualize and analyze all invalid values are plot as white (or blank) pixels.

Figure 8a shows the synthesized RGB picture of EPIC measurements at GMT time 00:17:51 on July 25, 2016. At this point in time the sun light covers most of the Pacific Ocean. In this figure, the white pixels represent cloud cover. Figure 8b shows the global COD (NASA ASDC L2 data), in which the white areas and colorful areas indicate the clear sky areas and cloudy areas, respectively. On the whole, the cloudy areas are consistent with the RGB image. The highlight (red) areas indicate that the cloud systems there contain optically heavy clouds. Figure 8c shows the A-band effective CTP (NASA ASDC L2 data), where the white areas indicate clear sky or no valid values, warm (brown) and cold (blue) color areas indicate high-level and low-level clouds, respectively. According to the A-band effective CTP, the high-level clouds are dominant in the equatorial area, and the low-level clouds play a major role in the cloud systems in the Northern Pacific area. Figure 8d and 8e show the baseline and retrieved CTP at A-band, respectively, which cloudy areas are consistent with the A-band effective CTP image on the whole. Due to the filtering setting in the CTP retrieval algorithm, there are more white pixels (invalid values) in these two figures. The difference of A-band retrieved CTP and A-band effective CTP is shown in Figure 8d. The A-band retrieved CTP is overall smaller than A-band effective CTP, which difference is within 100 mb. The highlighted (brown or red) areas are located in the high level clouds areas or large COD areas. This indicates that the complexity of cloud system has significant impact on the CTP retrieval. Figure 8g and 8h show the baseline and retrieved CTP in B-band respectively, which are similar to, but greater than the A-band. As shown in Figure 8i, the retrieved CTP at EPIC B-band is overall significantly larger than the retrieved CTP at EPIC A-band, which mean difference is up to 200 mb.
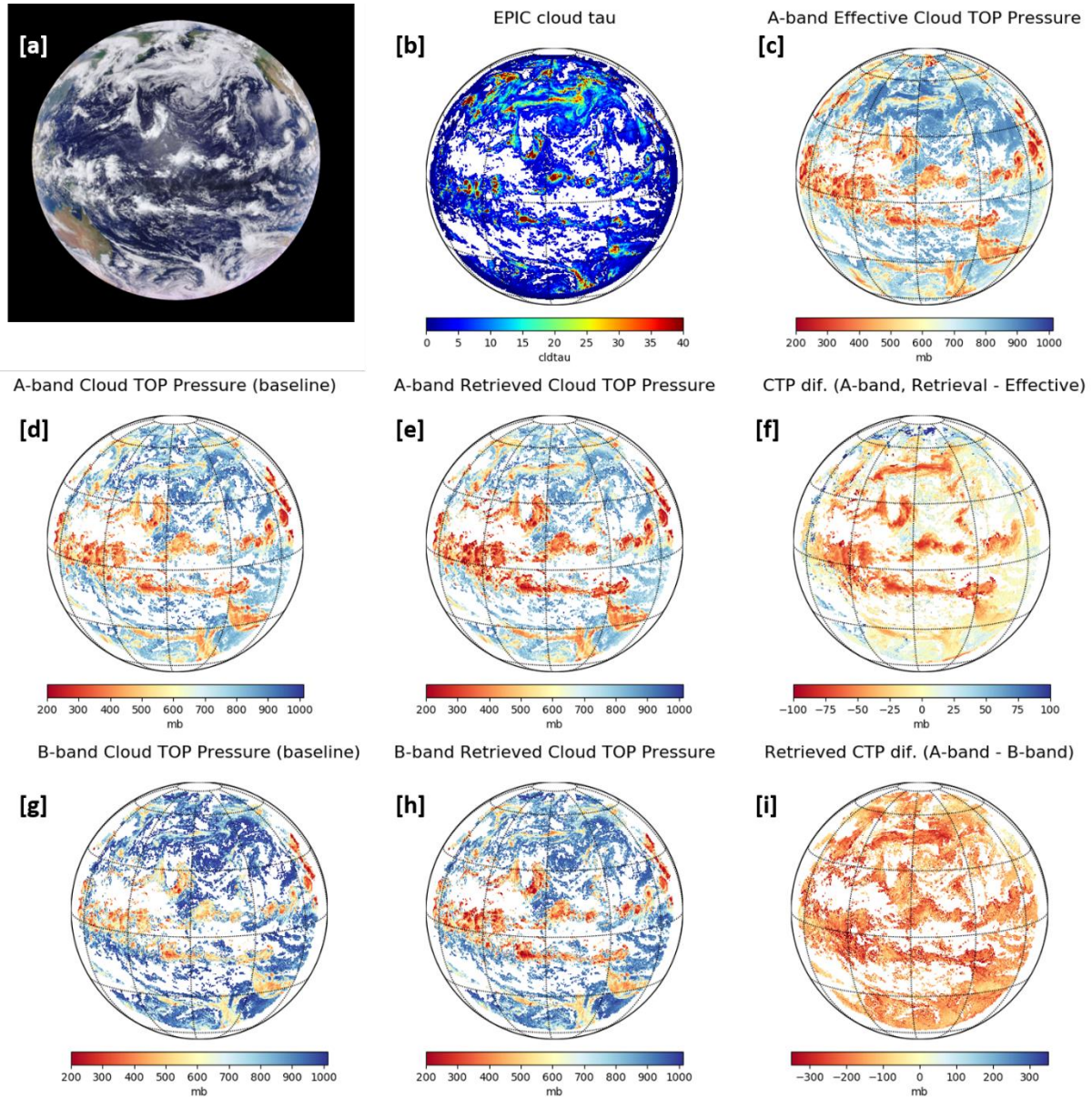
591

Figure 8. (a) RGB image from DSCOVR EPIC measurement at GMT time 00:17:51 on July 25, 2016; (b) and (c) COD (liquid assumption) and A-band effective CTP from NASA ASDC EPIC L2 products; (d) and (e) Baseline and retrieved CTP derived from EPIC A-band measurement; (f) the difference of A-band retrieved CTP and A-band effective CTP; (g) and (h) Baseline and retrieved CTP derived from EPIC B-band measurement; and (i) the difference of retrieved CTP between EPIC A-band and B-band.

As previously stated in the subsection 3.2: under single-layer cloud situations, the CTPs derived from EPIC A-band measurements have good agreement with the CTP from CALIPSO measurements; under multiple-layer cloud situations, the CTPs derived from EPIC measurements may be larger than the CTPs of high level thin-clouds due to the effect of photon penetration. Therefore, in the global range, for the large scale low-level stratus clouds, the retrieved CTPs from EPIC A-band measurements should agree well with the actual value of

22

605 CTPs, but for the complex cloud system with multiple-layer clouds, the CTPs derived from EPIC
606 A-band measurements may be larger than that of high level thin-clouds.

4. Conclusion

608   The in-cloud photon penetration has significant impacts on the CTP retrieval when using
609 DSCOVR EPIC oxygen A- and B- band measurements. To address this issue, we proposed two
610 methods, (1) the LUT based method and (2) the analytic transfer inverse model method for CTP
611 retrieval with consideration of in-cloud photon penetration. In the analytic transfer inverse model
612 method, we build an analytic equation that represents the reflection at TOA from above cloud,
613 in-cloud, and below-cloud, respectively. The coefficients of this analytic equation can be
614 derived from a series of EPIC simulations under different atmospheric conditions using a non-
615 linear regression algorithm. With EPIC observation data, the related solar zenith and sensor view
616 angle, surface albedo data, COD, and estimated cloud pressure thickness, we can retrieve the
617 CTP by solving the analytic equation.

618   We developed a package for the DSCOVR EPIC measurement simulation. The high
619 resolution radiation spectrum must be simulated first and then integrated with the EPIC filter
620 function in order to accurately simulate EPIC measurements. Because this process is highly time-
621 consuming, a polynomial fitting function is used when calculating the oxygen absorption
622 coefficients under different atmospheric conditions. At the same time, the double-k approach is
623 applied to do the high-resolution spectrum simulation to further reduce time-costs, which can
624 obtain high accuracy results with hundred-fold time reduction. The results of the EPIC
625 simulation measurements are consistent with theoretical analysis.

626   Based on the EPIC simulation measurements, we derived a series of coefficients from
627 various solar zenith angles for the analytic EPIC equations. Using these coefficients, we
628 performed CTP retrieval for real EPIC observation data. We have two kinds of retrieval results:
629 baseline CTP and retrieved CTP. The baseline CTP is similar to the effective CTP in Yang et al.,
630 (2019), which does not consider cloud penetration. The retrieved CTP is derived by solving the
631 analytic equation, with consideration of the in-cloud and below-cloud interactions. Compared to
632 the effective CTP provided by NASA ASDC L2 data, the baseline CTP value at A-band is
633 slightly higher, but the baseline CTP value at B-band is substantially higher. The retrieved CTP
634 for both oxygen A- and B- bands is smaller than the related baseline CTP. At the same time,
635 compared to the oxygen A-band, both baseline CTP and retrieved CTP at oxygen B-band is
636 larger. The cloud layer top pressure from CALIPSO measurements is used to validate the CTP
637 derived from EPIC measurement. Under single-layer cloud situations, the retrieved CTPs for
638 oxygen A-band agree well with the CTPs from CALIPSO, which mean difference is within 5 mb
639 in the case study. Under multiple-layer cloud situations, the CTPs derived from EPIC
640 measurements may be larger than the CTPs of high level thin-clouds due to the effect of photon
641 penetration.

642   Currently, this analytical transfer model method can only retrieve CTP, and it still need
643 cloud pressure thickness as an input parameter. However, in the satellite observations, both CTP
644 and cloud pressure thickness are unknown. The estimation or assumption of cloud pressure
645 thickness will bring in extra error in CTP retrieval. In the near future, we plan to address this
646 issue.

Reference

Bodhaine, B.A., Wood, N.B., Dutton, E.G. and Slusser, J.R.: On Rayleigh optical depth calculations. Journal of Atmospheric and Oceanic Technology, 16(11), pp.1854-1861, 1999.

Carbajal Henken, C. K., Doppler, L., Lindstrot, R., Preusker, R., and Fischer, J.: Exploiting the sensitivity of two satellite cloud height retrievals to cloud vertical distribution, Atmos. Meas. Tech., 8, 3419–3431, https://doi.org/10.5194/amt-8-3419-2015, 2015.

Chandrasekhar, S.: Radiative transfer. Dover, New York, 1960.

Chou, M.D. and Kouvaris, L.: Monochromatic calculations of atmospheric radiative transfer due to molecular line absorption. Journal of Geophysical Research: Atmospheres, 91(D3), pp.4047-4055, 1986.

Clough, S. A., Shephard, M. W., Mlawer, E. J., Delamere, J. S., Iacono, M. J., Cady-Pereira, K., Boukabara, S., and Brown, P.D.: Atmospheric radiative transfer modeling: a summary of the AER codes, Short Communication, J. Quant. Spectrosc. Ra., 91,233–244, 2005.

Daniel, J.S., Solomon, S., Miller, H.L., Langford, A.O., Portmann, R.W. and Eubank, C.S.: Retrieving cloud information from passive measurements of solar radiation absorbed by molecular oxygen and O2-O2. Journal of Geophysical Research: Atmospheres, 108(D16), 2003.

Dannenberg, Roger B.: Interpolation error in waveform table lookup, In Proceedings of the International Computer Music Conference. San Francisco: International Computer Music Association, 1998.

Davis, A.B., Merlin, G., Cornet, C., Labonnote, L.C., Riédi, J., Ferlay, N., Dubuisson, P., Min, Q., Yang, Y. and Marshak, A.: Cloud information content in EPIC/DSCOVR's oxygen A-and B-band channels: An optimal estimation approach. Journal of Quantitative Spectroscopy and Radiative Transfer, 216, pp.6-16, 2018a.

Davis, A.B., Ferlay, N., Libois, Q., Marshak, A., Yang, Y. and Min, Q.: Cloud information content in EPIC/DSCOVR's oxygen A-and B-band channels: A physics-based approach. Journal of Quantitative Spectroscopy and Radiative Transfer, 220, pp.84-96, 2018b.

685 Davis, A.B. and Marshak, A.: Space–time characteristics of light transmitted through dense
686 clouds: A Green's function analysis. Journal of the atmospheric sciences, 59(18), pp.2713-2727,
687 2002.

688 Duan, M., Min, Q. and Li, J.: A fast radiative transfer model for simulating high-resolution
689 absorption bands. Journal of Geophysical Research: Atmospheres, 110(D15), 2005.

690 Ferlay, N., Thieuleux, F., Cornet, C., Davis, A.B., Dubuisson, P., Ducos, F., Parol, F., Riédi, J.
691 and Vanbauce, C.: Toward new inferences about cloud structures from multidirectional
692 measurements in the oxygen A band: middle-of-cloud pressure and cloud geometrical thickness
693 from POLDER-3/PARASOL. Journal of Applied Meteorology and Climatology, 49(12),
694 pp.2492-2507, 2010.

695 Fischer, J. and Grassl, H.: Detection of cloud-top height from backscattered radiances within the
696 oxygen A band. Part 1: Theoretical study. Journal of Applied Meteorology, 30(9), pp.1245-1259,
697 1991.

698 Gastellu-Etchegorry, J.P., Gascon, F. and Esteve, P.: An interpolation procedure for generalizing
699 a look-up table inversion method. Remote Sensing of Environment, 87(1), pp.55-71, 2003.

700 Gelaro, R., McCarty, W., Suárez, M.J., Todling, R., Molod, A., Takacs, L., Randles, C.A.,
701 Darmenov, A., Bosilovich, M.G., Reichle, R. and Wargan, K.: The modern-era retrospective
702 analysis for research and applications, version 2 (MERRA-2). *Journal of Climate*, *30*(14),
703 pp.5419-5454, 2017.

704 Geogdzhayev, I. and Marshak, A.: Calibration of the DSCOVR EPIC visible and NIR channels
705 using MODIS Terra and Aqua data and EPIC lunar observations. Atmos. Meas. Tech. 11, 359 -
706 368, https://doi.org/10.5194/amt-11-359-2018, 2018

707 Gordon, I.E., Rothman, L.S., Hill, C., Kochanov, R.V., Tan, Y., Bernath, P.F., Birk, M., Boudon,
708 V., Campargue, A., Chance, K.V. and Drouin, B.J.: The HITRAN2016 molecular spectroscopic
709 database. Journal of Quantitative Spectroscopy and Radiative Transfer, 203, pp.3-69, 2017.

710 Holdaway, D. and Yang, Y.: Study of the effect of temporal sampling frequency on DSCOVR
711 observations using the GEOS-5 nature run results (Part II): Cloud Coverage. Remote
712 Sensing, 8(5), p.431, 2016.

713 Ishimaru, A.: Wave propagation and scattering in random media. Wiley-IEEE-Press, New York,
714 1999.

715 Irvine, W. M: The formation of absorption bands and the distribution of photon optical paths in a
716 scattering atmosphere. Bull. Astron. Inst. Neth., 17, 266–279, 1964.

717 Ivanov, V. V., and S. D. Gutshabash, 1974: Propagation of brightness wave in an optically thick
718 atmosphere. Phys. Atmos. Okeana, **10,** 851–863.
719 Koelemeijer, R.B.A., Stammes, P., Hovenier, J.W. and Haan, J.D.: A fast method for retrieval of
720 cloud parameters using oxygen A band measurements from the Global Ozone Monitoring
721 Experiment. Journal of Geophysical Research: Atmospheres, 106(D4), pp.3475-3490, 2001.

722 Kokhanovsky, A. A. and Rozanov, V. V.: The physical parameterization of the top of-
723 atmosphere reflection function for a cloudy atmosphere–underlying surface system: the oxygen

A-band case study, Journal of Quantitative Spectroscopy and Radiative Transfer, 85, 35–55, doi:10.1016/S0022-4073(03)00193-6, 2004.

Kokhanovsky, A. A., Rozanov, V. V., Zege, E. P., Bovesmann, H., and Burrows, J. P.: A semi analytical cloud retrieval algorithm usinfg backscattered radiation in 0.4–2.4 μm spectral region, J.Geophys. Res., 108, 4008, doi:10.1029/2001JD001543, 2003. Kuze, A. and Chance, K.V.: Analysis of cloud top height and cloud coverage from satellites using the O2 A and B bands. Journal of Geophysical Research: Atmospheres, 99(D7), pp.14481-14491, 1994.

Lelli L, Kokhanovsky, A.A., Rozanov, V.V., Vountas M., and Burrows, J.P.: Linear trends in cloud top height from passive observations in the oxygen A-band, Atmospheric Chemistry and Physics, 14, 5679-5692, doi:10.5194/acp-14-5679-2014, 2014.

Lelli L, Kokhanovsky, A.A., Rozanov, V.V., Vountas M., Sayer, A.M., and Burrows, J.P.: Seven years of global retrieval of cloud properties using space-borne data of GOME, Atmospheric Measurement Techniques, 5, 1551-1570, doi:10.5194/amt-5-1551-2012, 2012.

Loyola, D. G., Gimeno García, S., Lutz, R., Argyrouli, A., Romahn, F., Spurr, R. J. D., Pedergnana, M., Doicu, A., Molina García, V., and Schüssler, O.: The operational cloud retrieval algorithms from TROPOMI on board Sentinel-5 Precursor, Atmos. Meas. Tech., 11, 409–427, https://doi.org/10.5194/amt-11-409-2018, 2018.

Marshak, A., and Davis, A. (Eds.).: 3D radiative transfer in cloudy atmospheres. Springer Science & Business Media, 2005.

Marshak, A., Herman, J., Adam, S., Carn, S., Cede, A., Geogdzhayev, I., Huang, D., Huang, L.K., Knyazikhin, Y., Kowalewski, M. and Krotkov, N.: Earth observations from DSCOVR EPIC instrument. Bulletin of the American Meteorological Society, 99(9), pp.1829-1850, 2018.

Meyer, K., Yang, Y. and Platnick, S.: Uncertainties in cloud phase and optical thickness retrievals from the Earth Polychromatic Imaging Camera (EPIC). Atmospheric measurement techniques, 9(4), p.1785, 2016.

Min, Q. and Harrison, L.C.: Retrieval of atmospheric optical depth profiles from downward-looking high-resolution O2 A-band measurements: Optically thin conditions. Journal of the atmospheric sciences, 61(20), pp.2469-2477, 2004..

Min, Q., Yin, B., Li, S., Berndt, J., Harrison, L., Joseph, E., Duan, M. and Kiedron, P.: A high-resolution oxygen A-band spectrometer (HABS) and its radiation closure. Atmospheric Measurement Techniques, 7(6), pp.1711-1722, 2014.

O'brien, D.M. and Mitchell, R.M.: Error estimates for retrieval of cloud-top pressure using absorption in the A band of oxygen. Journal of Applied Meteorology, 31(10), pp.1179-1192, 1992.

Pandey, P., Ridder, K.D., Gillotay, D. and Van Lipzig, N.P.M.: Estimating cloud optical thickness and associated surface UV irradiance from SEVIRI by implementing a semi-analytical cloud retrieval algorithm. Atmospheric Chemistry and Physics, 12(17), pp.7961-7975, 2012.

Preusker, R. and Lindstrot, R.: Remote Sensing of Cloud-Top Pressure Using Moderately Resolved Measurements within the Oxygen A Band-A Sensitivity Study, J. Appl. Meteorol. Clim., 48, 1562–1574, 2009.

764 Richardson, M. and Stephens, G.L.: Information content of OCO-2 oxygen A-band channels for
765 retrieving marine liquid cloud properties. *Atmospheric Measurement Techniques*, *11*(3),
766 pp.1515-1528, 2018.

767 Rozanov, V. V. and Kokhanovsky, A. A.: Semianalytical cloud retrieval algorithm as applied to
768 the cloud top altitude and the cloud geometrical thickness determination from top-of-atmosphere
769 reflectance measurements in the oxygen A band, Journal of Geophysical Research:
770 Atmospheres, 109, 4070, doi:10.1029/2003JD004104, 2004.

771 Schuessler, O., Rodriguez, D.G.L., Doicu, A. and Spurr, R.: Information Content in the Oxygen
772 A-Band for the Retrieval of Macrophysical Cloud Parameters. IEEE Transactions on Geoscience
773 and Remote Sensing, 52(6), pp.3246-3255, 2013.

774 Seager, S., Turner, E.L., Schafer, J. and Ford, E.B.: Vegetation's red edge: a possible
775 spectroscopic biosignature of extraterrestrial plants. Astrobiology, 5(3), pp.372-390, 2005.

776 Stamnes, K., Tsay, S.C., Wiscombe, W. and Jayaweera, K.: Numerically stable algorithm for
777 discrete-ordinate-method radiative transfer in multiple scattering and emitting layered
778 media. Applied optics, 27(12), pp.2502-2509, 1988.

779 Thomas, G. E., and Stamnes, K.: Radiative transfer in the atmosphere and ocean. Cambridge
780 University Press, Cambridge, 2002.

781 Tilstra, L.G., Wang, P. and Stammes, P.: Surface reflectivity climatologies from UV to NIR
782 determined from Earth observations by GOME-2 and SCIAMACHY. Journal of Geophysical
783 Research: Atmospheres, 122(7), pp.4084-4111, 2017.

784 Van de Hulst, H. C.: Multiple Light Scattering: Tables, Formulas, and Applications. Academic
785 Press, 299 pp, 1980.

786 Van de Hulst HC.: Multiple light scattering: tables, formulas, and applications. Elsevier;
787 2012.Yamamoto, G. and Wark, D. Q.: Discussion of letter by A. Hanel: determination of cloud
788 altitude from a satellite, Journal of Geophysical Research: Atmospheres, 66, 3596, 1961.

789 Vaughan, M.A., Young, S.A., Winker, D.M., Powell, K.A., Omar, A.H., Liu, Z., Hu, Y. and
790 Hostetler, C.A.: November. Fully automated analysis of space-based lidar data: An overview of
791 the CALIPSO retrieval algorithms and data products. In *Laser radar techniques for atmospheric
792 sensing* (Vol. 5575, pp. 16-30). International Society for Optics and Photonics, 2004.

793 Yang, Y., Marshak, A., Mao, J., Lyapustin, A. and Herman, J.: A method of retrieving cloud top
794 height and cloud geometrical thickness with oxygen A and B bands for the Deep Space Climate
795 Observatory (DSCOVR) mission: Radiative transfer simulations. Journal of Quantitative
796 Spectroscopy and Radiative Transfer, 122, pp.141-149, 2013.

797 Yang, Y., Meyer, K., Wind, G., Zhou, Y., Marshak, A., Platnick, S., Min, Q., Davis, A.B.,
798 Joiner, J., Vasilkov, A. and Duda, D.: Cloud products from the Earth Polychromatic Imaging
799 Camera (EPIC): algorithms and initial evaluation. Atmospheric Measurement Techniques, 12(3),
800 2019.

801